Green Chemistry

PAPER

View Article Online
View Journal | View Issue

Cite this: *Green Chem.*, 2018, **20**, 3867

Scalable thin-layer membrane reactor for heterogeneous and homogeneous catalytic gas–liquid reactions†

Yiming Mo, ‡ Joseph Imbrogno, ‡ Haomiao Zhang and Klavs F. Jensen *

Catalytic gas–liquid reactions have potential as environmentally benign methods for organic synthesis, particularly hydrogenation and oxidation reactions. However, safety and scalability are concerns in the application of gas–liquid reactions. In this work, we develop and demonstrate a scalable, sustainable, and safe thin-layer membrane reactor for heterogeneous Pd-catalyzed hydrogenations and homogenous Cu(I)/TEMPO alcohol oxidations. The implementation of a Teflon amorphous fluoroplastic (AF) membrane and porous carbon cloth in the membrane reactor provides sufficient gas–liquid mass transfer to afford superior performance compared to conventional packed-bed or trickle-bed reactors. The membrane separates the gas from the liquid, which avoids the formation of explosive mixtures for oxygenation reactions and simplifies the two-phase hydrodynamics to facilitate scale-up by stacking modules, while significantly reducing gas consumption. In addition, 3-dimensional simulations deliver insights into the mass transfer and hydrodynamic behavior to inform optimal membrane reactor design and operation.

Received 19th June 2018,
Accepted 23rd July 2018

DOI: 10.1039/c8gc01917g

rsc.li/greenchem

Introduction

Among numerous pharmaceutical transformations, gas–liquid reactions, such as hydrogenation,[1] aerobic oxidation,[2,3] and ozonolysis,[4] show attractive atom economy in comparison to other chemical transformations. For example, direct hydrogenation of pharmaceutical precursors with hydrogen gas outpaces other costly sacrificial reducing reagents, such as hydrides ($LiAlH_4$ and $NaBH_4$) or borane reagents. In addition to atom economy, the general availability of gaseous reagents and facile downstream separation make gas–liquid reactions potential green chemistry processes.[5] However, concerns of process efficiency, scalability, and safety of gas–liquid systems create barriers for pharmaceutical applications and this becomes even more challenging when heterogeneous catalysts are present in gas–liquid systems.[1,6]

Over the past decade, continuous flow technology has emerged as a powerful technique to produce active pharmaceutical ingredients (APIs) driven by advantages of continuous technology over conventional batch or semi-batch processes, including steady state operation, enhanced heat and mass transfer rates, reproducibility, and improved safety and process reliability.[7–12] These benefits are especially true for gas–liquid reaction systems, where the absence of high-pressure headspace gas and reduced reactor volume of continuous flow reactors significantly improve the safety profiles compared to high-pressure reaction vessels. In addition, the increased interfacial area per volume in flow reactors accelerates multiphase mass transfer rates.

Packed-bed reactors, a common type of gas–liquid reactor, despite their mature development in the petrochemical industry, have not been widely adopted in pharmaceutical manufacturing.[13] Zaborenko *et al.* studied packed-bed reactors of small scale (20 g catalyst), medium scale (120 g catalyst), and pilot scale (1.5 kg catalyst) for successful development of continuous hydrogenation of a pharmaceutical intermediate.[13] Yang *et al.* provided in-depth characterization of the micro-packed-bed reactor to establish a fundamental understanding of the multiphase hydrodynamics and mass transfer properties.[1]

The complex multiphase hydrodynamics in packed-bed reactors requires extensive understanding of the system behavior across different scales. Additionally, direct contact of gas and liquid is unfavorable for aerobic oxidations due to the formation of flammable oxidant and organic solvent mixtures.[6] The low cross-tube heat transfer of packed-bed reactors can also lead to a non-uniform temperature profile for highly exothermic reactions, leaving APIs with temperature-sensitive functional groups at risk for degradation.

Department of Chemical Engineering, Massachusetts Institute of Technology, Cambridge, MA 02139, USA. E-mail: kfjensen@mit.edu

†Electronic supplementary information (ESI) available. See DOI: 10.1039/c8gc01917g

‡These authors contributed equally to this work.

Recently, Gavriilidis *et al.* demonstrated heterogeneously catalyzed benzyl alcohol oxidation in a ceramic membrane packed-bed reactor.[14] However, the pressure-driven mechanism of the ceramic membrane has no selectivity over gas and liquid permeation, leading to difficulty in operating under desired two-phase pressure profile. Ley *et al.* proposed and demonstrated the concept of a tube-in-tube reactor using gas-permeable Teflon amorphous fluoroplastic (AF) membranes for various gas–liquid reactions, including heterogeneous and homogeneous hydrogenation,[15] ozonolysis,[4] and carboxylation.[16] The implementation of Teflon AF membrane (highly permeable to gas phase and impermeable to liquid phase) greatly simplifies the reactor operation compared to ceramic membrane. The capabilities and physical properties of the Teflon AF membrane have been described elsewhere.[17–20] Yang *et al.* used both analytical and numerical methods to understand the behavior of the tube-in-tube reactor, and indicated challenges in scale-up due to radial-diffusion-limited mass transfer.[21] The challenge of incorporating heterogeneous catalysts in a tube-in-tube reactor makes it less attractive for a broad category of heterogeneous catalytic gas–liquid reactions.

Thus, an efficient, safe, scalable, and widely applicable continuous flow reactor design for gas–liquid reactions is still desirable for low-volume applications. Here, we present a scalable, sustainable, and safe thin-layer membrane reactor for heterogeneous and homogenous catalytic gas–liquid reactions. The reactor uses a Teflon AF membrane sandwiched between two sheets of thin-layer carbon cloth, which enables superior gas–liquid mass transfer performance. The carbon cloth layer works as a heterogeneous catalyst support, making this reactor design applicable for heterogeneous catalytic gas–liquid reactions. Additionally, nearly all of the gas is consumed by the reaction, removing the need for recycle and increasing the safety of operation by minimizing the amount of gas required. The membrane reactor is demonstrated using common heterogeneous Pd-catalyzed hydrogenations and homogeneous Cu(I)/TEMPO aerobic alcohol oxidations. The membrane reactor is also stackable allowing for scale-up. In-depth modeling of the membrane reactor affords fundamental understanding and design principles for application to various gas–liquid reactions with different kinetics.

Experimental section

Materials and reagents

Woven carbon cloth with palladium and platinum catalyst was purchased from Fuel Cell Store. Teflon AF membrane (40 μm thick) was purchased from Biogeneral. Nitrobenzene, 2-ethyl cinnamate, 10-undecyn-1-ol, benzyl alcohol, 3-phenyl-1-propanol, furfuryl alcohol, tetrakisacetonitrile copper(I) triflate $Cu(MeCN)_4(OTf)$, 2,2′-bipyridine, 1-methylimidazole (NMI), and (2,2,6,6-tetramethylpiperidin-1-yl)oxyl (TEMPO) were purchased from Sigma-Aldrich and used without further purification. Hydrogen (99.999%), oxygen (99.99%), and nitrogen (99.999%) were purchased from Airgas.

Thin-layer membrane reactor design

A Teflon AF membrane was sandwiched between two sheets of woven carbon cloth (Fig. 1a) with the gas and liquid phases flowing separately through the two porous carbon cloth layers. The unique property of Teflon AF membranes (highly permeable to gas phase and impermeable to liquid phase) offers the capability of separating the two phases while allowing gas to diffuse through the membrane into the liquid phase. The design was engineered to minimize the thickness of the combined assembly (carbon cloth: 300 μm and Teflon AF membrane: 40 μm) in order to reduce the gas molecule diffusion length and improve the mass transfer performance. The reactor volume of liquid side is 0.05 ml (carbon cloth dimensions: 30 mm × 13 mm × 0.3 mm, porosity: 43%).

For demonstration purposes, the membrane reactor (Fig. 1b and c) was fabricated out of aluminum, due to the lower material cost. The membrane reactor can also be coated with

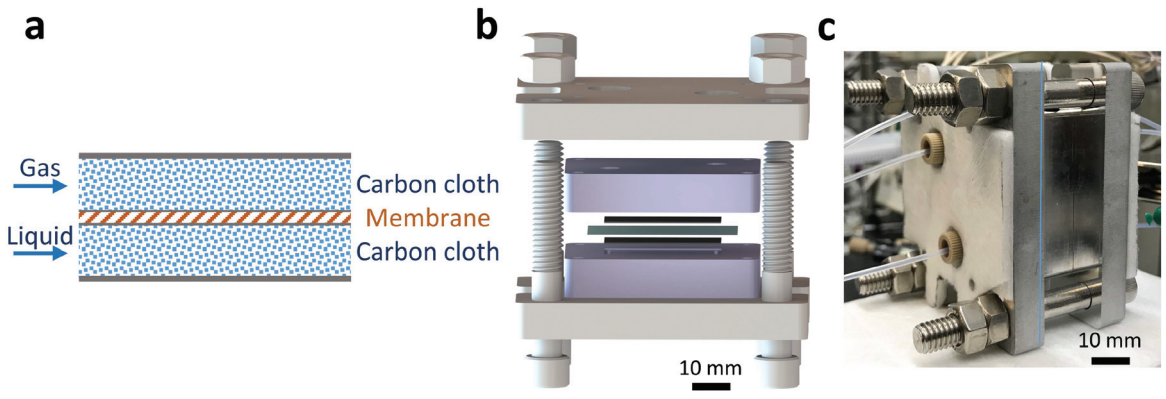

Fig. 1 (a) Gas–liquid membrane reactor schematics: Teflon AF membrane sandwiched between two sheets of carbon cloth layers to offer separation of gas and liquid while allowing the gas phase to diffuse through the membrane to react in the liquid phase. (b) Exploded-view CAD drawing of the gas–liquid membrane reactor. Two thin black layers are carbon cloth, and the thin blue layer is a Teflon AF membrane. (c) Photograph of assembled single-layer membrane reactor.

perfluoroalkoxy alkane (PFA) or fabricated out of 316 stainless steel for better chemical compatibility. The cartridge heaters inside the reactor combined with a proportional–integral–derivative (PID) temperature controller kept the membrane reactor at the desired reaction temperature.

General membrane reactor operating procedures

General start-up procedure. Prior to each experiment, the system was rinsed with appropriate liquid solvent on the liquid side and nitrogen on the gas side. The liquid side was then filled with the liquid reagent stream, and the gas side was adequately purged by the gas reagent. The gas side was pressurized while maintaining a small (~150 kPa) transmembrane pressure with the back-pressure regulator (BPR) on the liquid side, which is necessary to prevent gas from passing through the BPR and avoid rupturing the membrane. The reaction gas flow was controlled using a mass flow controller (MFC, Brooks Instrument 5850i) and the BPR was pressurized using nitrogen gas controlled by a pressure controller (Alicat Scientific).

General reaction procedure. Once the gas side pressure had reached the appropriate pressure set-point, the temperature controller was turned on and the liquid flow was started. The reagent stream was degassed before entering the reactor. The system was purged with three reactor volumes in order to reach steady state before sample collection. Reaction parameters, such as temperature and flow rate, were varied to collect samples under different reaction conditions. Samples were analyzed with gas chromatography (GC, Agilent 6890).

General shut-down procedure. The liquid and gas flow rates were stopped. Then, simultaneously, the BPR pressure was reduced to atmospheric pressure and the gas and liquid outlets were switched to venting positions, allowing for safe de-pressurization of the system and avoiding membrane rupture. After every experiment, the system was flushed with the same solvent used during the experiment on the liquid side and nitrogen on the gas side. Additional details, including assembly procedure and images of the process control equipment, are shown in the ESI (Fig. S6).†

Results and discussion

Heterogeneous catalytic hydrogenations

Direct H_2 hydrogenation reactions with heterogeneous catalysts are attractive chemical transformations for synthesis because of their atom economy and easy-to-reuse heterogeneous catalysts.[5] However, the major challenge for H_2 heterogeneous hydrogenations is the poor solubility of H_2 in the organic solvent coupled with the slow mass transfer rate from the gas phase to the liquid phase and the catalyst surface. The thin-layer membrane reactor design minimizes the diffusion distance for H_2 molecules to the reactive catalyst surface in order to maximize the mass transfer performance. In addition, the membrane reactor was engineered for high pressure operation (tested up to 3.1 MPa), which improves the solubility of H_2 in the organic solvent, intensifying the hydrogenation process.

To investigate the potential of the membrane reactor in heterogeneous catalysis, we began our investigation with hydrogenation of nitrobenzene **1a** to aniline **1b** with cost-effective carbon cloth embedded with platinum (Pt) or palladium (Pd) as the heterogeneous catalyst (commercially available from Fuel Cell Store, ~$1/cm^2) (Table 1). The loading of the catalyst on the carbon cloth for both Pt and Pd catalysts was 4 mg cm^{-2} (based on carbon cloth surface area: width × length). The Pt catalyst was too aggressive, leading to extensive formation of the over-reduction product, while Pd showed a better selectivity towards the desired product **1b** compared to Pt (Table 1, entries 1 and 2). Increasing the residence time from 0.5 min to 1 min did not show significant improvement of yield of **1b** (Table 1, entries 2 and 3).

With the optimal catalyst (Pd), the heterogeneous catalytic hydrogenation scope was expanded to other substrates (Table 2). The reduction of C–C double and triple bonds is facile under these optimized reaction conditions (full conversion of the starting material). In order to keep the theoretical hydrogen consumption per reagent volume the same, the concentration of the reagent was determined based on the number of hydrogen molecules needed per reagent molecule.

Table 1 Optimization of heterogeneous hydrogenation of nitrobenzene **1a** to aniline **1b**[a]

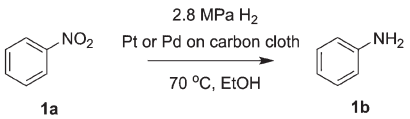

No.	Catalyst	RT[b] (min)	1a	Intermediates	Over-reduction	1b
1	Pt	0.5	19%	20%	11%	50%
2	Pd	0.5	3%	7%	5%	85%
3	Pd	1	2%	5%	7%	86%

[a] 0.2 M **1a** in ethanol (EtOH). [b] RT: residence time.

Table 2 Heterogeneous hydrogenation substrate scope[a]

No.	Substrate	Product	RT (min)	T (°C)	Yield
1[b]	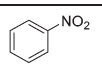 1a	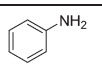 1b	0.5	70	85%
2[c]	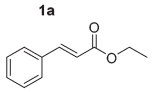 2a	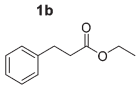 2b	0.5	50	94%
3[d]	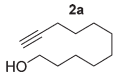 3a	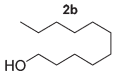 3b	0.5	50	95%

[a] Hydrogen pressure: 2.8 MPa. [b] 0.2 M **1a** in EtOH. [c] 0.6 M **2a** in ethyl acetate. [d] 0.3 M **3a** in ethyl acetate.

All substrates achieved excellent yields with the optimized hydrogenation conditions (Table 2, entries 1–3).

Homogeneous Cu/TEMPO catalyzed aerobic alcohol oxidations

Recent developments of aerobic oxidation reactions provide attractive alternatives to conventional approaches employing stoichiometric oxidants.[22–24] However, the practical usage of aerobic oxidation in large-scale synthesis raises safety concerns, namely the formation of explosive mixtures (flammable organic solvents in oxygen). A number of microreactor-based biphasic flow implementations of aerobic oxidation improve the safety profile by accurately controlling oxygen flow in the microchannels.[25,26] However, the explosive mixtures are still present in the microreactor system. Tube-in-tube membrane reactors show great potential to avoid the formation of explosive mixtures, but still have inherent scalability issues for large-scale synthesis.[21,27] Implementing the thin-layer membrane reactor designed in this work offers the opportunity to make the aerobic oxidation reactions both safe and scalable for industrial applications.

Instead of using a catalyst-embedded carbon cloth layer, pristine carbon cloth was installed in the membrane reactor, along with the same Teflon AF membrane to accommodate the homogeneous catalytic aerobic oxidation. Cu/TEMPO catalyzed oxidation of alcohols is an efficient approach to selective aldehyde synthesis.[22] This reaction was demonstrated to have first-order kinetics on oxygen concentration in the solvent, which directly corresponds to the oxygen pressure in the gas phase. The ability to handle high pressures in the membrane reactor would intensify this reaction by orders of magnitude compared to batch processing. Meanwhile, the Teflon AF membrane separates the oxygen and organic solvent to circumvent the formation of explosive mixtures.

Three substrates (**4a–6a**) were examined in the membrane reactor with optimized conditions, and all products were achieved in excellent yields (Table 3). The residence times required to reach full conversion were around 1 min, significantly shorter than the several-hour reaction times required under batch conditions.[22]

Table 3 Homogeneous Cu/TEMPO catalyzed aerobic alcohol oxidation substrate scope[a]

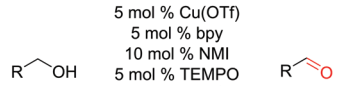

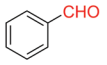

4b
100%
0.8 MPa 30 °C
r.t. = 0.5 min

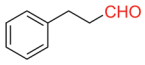

5b
100%
2.7 MPa 50 °C
r.t. = 1 min

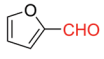

6b
100%
2.7 MPa 30 °C
r.t. = 0.5 min

[a] 0.2 M alcohol substrate with 0.05 equiv. Cu(OTf), 0.05 equiv. 2,2′-bipyridyl (bpy), 0.1 equiv. 1-methylimidazole (NMI), and 0.05 equiv. TEMPO dissolved in MeCN.

Gas purge for oxygenation reactions

Even though the explosive mixture of liquid organic solvents and oxygen is avoided in the membrane reactor for oxygenation reactions, the organic solvent vapors could potentially penetrate through the Teflon AF membrane to the gas side, which raises safety concerns for large-scale applications. Unlike hydrogenation reactions in the membrane reactor, where the gas side outlet is plugged to reduce the unnecessary hydrogen consumption, an additional oxygen purge stream is required to avoid the accumulation of organic solvent vapors in the gas side, which could exceed lower explosive limits under certain reaction conditions.

In order to ensure safe operation of the membrane reactor for reactions involving oxygen, the required oxygen purge stream flowrate needed to keep the solvent vapor concentration under the lower explosive limit (LEL) was calculated for various reaction temperatures and organic solvents. Since the LEL data of organic solvents in pure oxygen are rarely available, the approach developed by Chen[28] for estimating the LEL in pure oxygen with the LEL in air was used. The gas purge stream flowrate can be obtained using the permeability of organic solvent vapors through the Teflon AF membrane[29,30] and LEL in pure oxygen (eqn (1)) (see ESI† for detailed derivations).

$$\text{Flowrate} = D \cdot A_{\text{mem.}} \frac{C_{\text{sat}}}{d_{\text{mem}}} \left(1 - \frac{\text{LEL}_{\text{air}} \times p}{p_{\text{sat}}}\right) / C_{\text{sol}} \quad (1)$$

$$C_{\text{sol}} = r_{\text{safety}} \times \text{LEL}_{\text{O}_2} \times \frac{p}{\text{RT}} \quad (2)$$

where D is the diffusion coefficient of the organic solvent molecule in the Teflon AF membrane, A_{mem} is the surface area of the membrane, C_{sat} is the saturated organic solvent concentration in the gas phase, d_{mem} is the thickness of the membrane, p is the absolute pressure in the gas side, and p_{sat} is the saturated organic solvent partial pressure. C_{sol} is the safe organic solvent concentration level in the gas phase, which is determined with eqn (2). r_{safety} is the safety ratio with a value ranging from 0 to 1, which is selected based on desired certainty of safe operation.

Fig. 2 shows the required gas purge stream flowrates for four solvents under various reaction temperatures with a safety ratio of 0.5 (0.5 is selected as a medium value between 0 and 1, and the actual value can be determined based on desired safety level). Reaction temperature plays an important role in determining the required purge stream, since temperature has an impact on the diffusion coefficient, saturated solvent vapor pressure, and solvent solubility in membrane. For all solvents studied, a purge stream is not required if the reaction is carried out under 40 °C. Acetone requires a very large purge stream to keep the solvent vapor concentration under C_{sol} due to its low LEL, low boiling point and high diffusion coefficient. Cyclohexane, even with the lowest LEL, requires a small purge stream because of its high boiling point and low diffusion coefficient. Methanol and ethanol, with relatively high LEL values, high boiling points, and low diffusion coefficients,

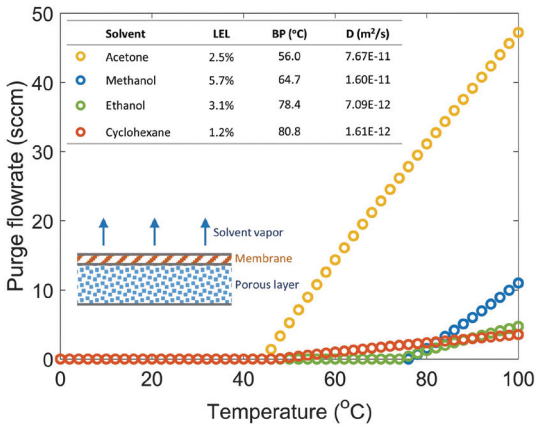

Fig. 2 Required purge stream flowrates for various reaction temperatures and solvents. The inserted table shows the LELs in pure oxygen, boiling points (BP), and diffusion coefficients at 25 °C of the studied solvents.

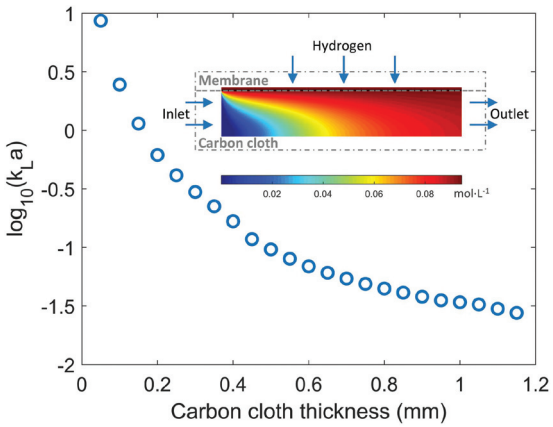

Fig. 3 The mass transfer coefficient k_La values under various carbon cloth thicknesses. Insert figure: the hydrogen concentration profile in the membrane and carbon cloth (membrane thickness is 40 μm, and carbon cloth thickness is 0.6 mm).

require no purge stream up to 75 °C, appearing to be the two safest solvents among the solvents studied.

For oxygenation reactions, implementing a safe solvent (*e.g.* methanol and ethanol) and operating under a low reaction temperature are essential to improve the safety profile of the membrane reactor, otherwise a purge stream is required to avoid the accumulation of the penetrated organic solvent vapor in the gas side.

Membrane reactor design optimization

Gas molecules have such a high permeability through the thin Teflon AF membrane that the dominant gas mass transfer resistance is in the liquid layer.[21] Hence, the mass transfer performance of the membrane reactor mainly depends on the thickness of the carbon cloth layer, which also determines the reactor volume if the same membrane area is used. A thin carbon cloth layer is favourable when the reaction is mass transfer limited, while kinetically limited reactions would require a thicker carbon cloth layer (large reactor volume) to increase the residence time. In order to maximize the productivity of the membrane reactor with the same membrane area, the optimal thickness of the carbon cloth layer needs to be determined according to relative ratio of mass transfer rate and reaction rate.

Understanding and calculating the mass transfer coefficient k_La in the membrane reactor provides the basis for comparison with other typical gas–liquid–solid reactor configurations (*e.g.* trickle-bed or packed-bed reactors). COMSOL simulation of hydrogen mass transfer into ethanol under various carbon cloth thicknesses was conducted. As shown in Fig. 3, the mass transfer performance strongly depends on the thickness of the carbon cloth layer ranging across two orders of magnitude. The hydrogen concentration profile in the membrane is nearly homogeneous indicating negligible mass transfer resistance in the membrane, which is consistent with reported results.[21] The thin-layer membrane reactor with a carbon cloth thickness of 0.3 mm used in the previous experiments has a k_La value of 0.3 s^{-1}. Even a relatively thick carbon cloth (>1 mm) has a k_La value on the order 10^{-2}–10^{-1} s^{-1}, which is comparable to the k_La values (0.01–0.08 s^{-1}) reported for conventional laboratory-scale trickle-bed reactors.[31] In addition to the superior mass transfer performance, it is also tunable by changing the carbon cloth thickness according to the kinetics of the reaction system.

The porous structure of the carbon cloth helps the flow distribution across the reactor and makes the flow profile close to that of plug flow (Fig. S8†), which simplifies the hydrodynamics making it possible to understand the system with a one-dimensional (1D) model. The 1D model identifies two dimensionless numbers, first Damköhler number (Da_I) and second Damköhler number (Da_{II}), that control the reaction outcome of the membrane reactor (see ESI† for detailed derivation).

$$Da_I = k\tau \quad (3)$$

$$Da_{II} = \frac{k}{k_La} \quad (4)$$

where k represents the kinetic rate constant, τ is the residence time, and k_La is the mass transfer coefficient. Da_I denotes the residence time *versus* the reaction time scale, which can roughly indicate the reaction conversion for homogeneous singe-phase reaction. Da_{II} is introduced due to the diffusion of gas through membrane and liquid phase, which represents the ratio between diffusion time scale and reaction time scale. The interplay among these three time scales determines the reaction conversion in the membrane reactor.

COMSOL 3D simulation illustrates the dependence of reaction outcome on different values of Da_I and Da_{II} (Fig. 4). When $Da_{II} \ll 1$, indicating the reaction rate is much slower than the diffusion rate, the reaction conversion in the membrane reactor is insensitive to the value of Da_{II}, corresponding to the "reaction limited" regime in Fig. 4. In contrast, the depen-

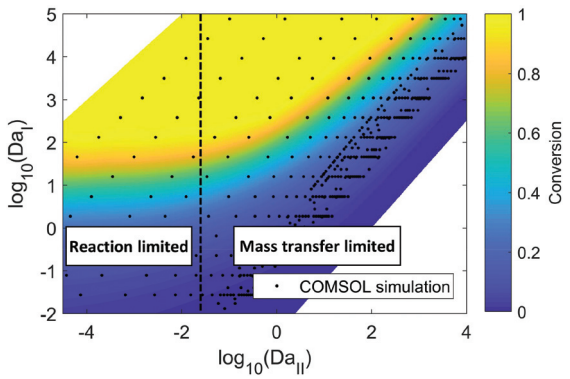

Fig. 4 COMSOL simulation of hydrogenation of nitrobenzene with ethanol as solvent in the membrane reactor. The residence time, carbon cloth thickness, and reaction kinetic constant are varied to obtain different values of Da_I and Da_{II}. Hydrogenation pressure: 2.8 MPa. Carbon cloth layer dimension: length (30 mm) × width (12 mm) × thickness (0.05 mm–3 mm). Membrane thickness: 40 μm. The reaction kinetics are available from reported literature, and changing the kinetic constant corresponds to the change of catalyst loading or reaction temperature.[32]

dence of the reaction conversion on Da_{II} becomes much stronger when $Da_{II} > 1$, corresponding to the "mass transfer limited" regime, where an efficient mass transfer configuration is beneficial for reaction conversion. Thus, identifying the ratio between mass transfer time scale and reaction time scale is essential for choosing the optimal membrane reactor design (*i.e.* carbon cloth layer thickness) in order to balance the trade-off between productivity and reactor fabrication cost.

Scale-up of thin-layer membrane reactor

The complex process needed to scale up conventional trickle-bed or packed-bed reactors is mainly attributed to the change in multiphase hydrodynamics, mass, and heat transfer properties across different scales.[13] The simplified fluid hydrodynamics in the thin-layer membrane reactor offers the opportunity for straightforward scale-up with a stackable design. The stackable design maintains a fixed heat and mass transfer distance (carbon cloth thickness) while increasing the reactor size laterally and in parallel, resulting in preserved heat and mass transfer advantages of the single-layer membrane reactor while meeting the required productivity. As shown in Fig. 5a, the main channels of a 3-layer stacked membrane reactor distribute or collect gas streams and liquid streams into or from each layer. The design of distribution channels follows barrier-based uniform flow distribution criteria.[33,34] Fig. 5b shows an assembled 3-layer membrane reactor, and each layer has identical inner dimensions as the single-layer membrane reactor. If the reaction is highly exothermic requiring fast heat dissipation, multiple cooling layers could be implemented between two individual layers periodically to maximize the heat dissipation rate (Fig. S12†).

In order to enable direct scale-up from a single-layer to multiple-layers, it is essential to have identical flow distribution

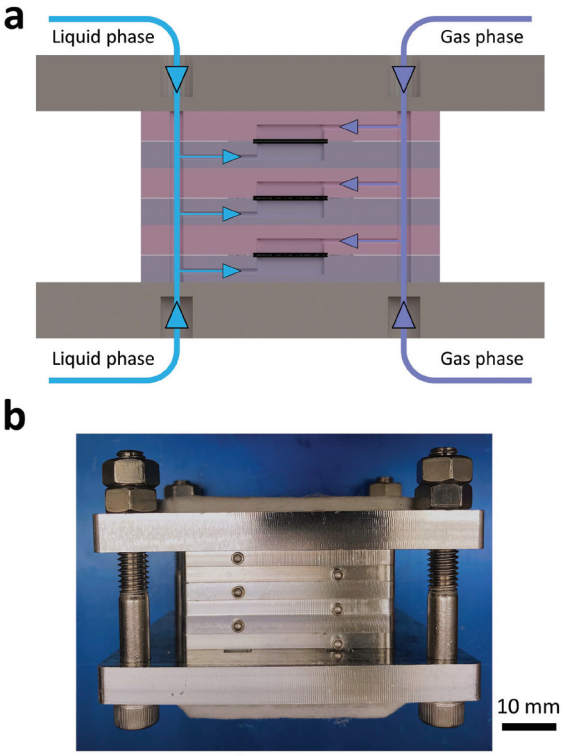

Fig. 5 (a) Cross-section of the inlet channels in a 3-layer stacked membrane reactor with blue arrows indicating the liquid flow and purple arrows indicating the gas flow. The outlet channels collect flow from each layer with reversed arrow directions. (b) Photo of a 3-layer stacked membrane reactor.

across each layer in the stacked membrane reactor. Besides the optimized distribution channel design shown in Fig. 5a, the porous carbon cloth in each layer also plays an important role in unifying flow distribution. COMSOL hydrodynamics simulations (Fig. S13 and S14†) illustrate the difference of flow distribution with and without carbon cloth for 3-layer and 10-layer membrane reactors (Table 4). Compared to the case without carbon cloth, the porous structure of the carbon cloth adjusts the flow pressure drop profile, which helps to maintain an even distribution of flow from the main channel. This effect becomes more important as an increasing number of layers are stacked together.

The 3-layer membrane reactor (Fig. 5b) was demonstrated using the hydrogenation of ethyl cinnamate (**2a**). Using identi-

Table 4 The coefficient of variation[a] for flow distribution with and without carbon cloth in a 3-layer and 10-layer membrane reactor[b]

	3-Layer	10-Layer
With carbon cloth	0.05%	0.14%
Without carbon cloth	0.61%	6.45%

[a] Coefficient of variation is the ratio between standard deviation and average. [b] Only the flow distribution of liquid is considered. Gas flow distribution is typically uniform due to the low viscosity of gas.

cal reaction conditions as the single-layer membrane reactor, (Table 2, entry 2) except for 0.3 ml min^{-1} liquid flowrate (0.1 ml min^{-1} in the single-layer membrane reactor), the 3-layer membrane reactor was able to produce 1.9 g h^{-1} of the hydrolyzed product in 91% yield continuously, tripling the hydrogenation productivity without any reaction condition optimization.

Conclusion

This work presented the development and experimental validation of a thin-layer membrane reactor with commonly used heterogeneous Pd-catalyzed hydrogenations and homogeneous Cu(I)/TEMPO aerobic alcohol oxidations. The unique structure implemented a Teflon AF membrane and porous carbon cloth in the membrane reactor to separate the gas from the liquid, simplifying the multiphase hydrodynamics for predictable reactor performance and straightforward scale-up. The thin-layer design minimized mass transfer resistance in gas–liquid systems. Optimizing the carbon cloth thickness according to the reaction kinetics balanced the trade-off between reactor manufacturing cost and productivity. Both the membrane design and the detailed guidelines for safe operation of oxygenation reactions provided in this work could potentially accelerate the adoption of oxygen and hydrogen as cheap, green reagents in industrial applications. In addition, a stackable membrane design demonstrated a possible scale-up strategy.

Conflicts of interest

There are no conflicts to declare.

Acknowledgements

We thank the Novartis-MIT Center for Continuous Manufacturing for financial support.

References

1 C. Yang, A. R. Teixeira, Y. Shi, S. C. Born, H. Lin, Y. L. Song, B. Martin, B. Schenkel, M. P. Lachegurabi and K. F. Jensen, *Green Chem.*, 2018, **20**, 886–893.
2 D. P. Hruszkewycz, K. C. Miles, O. R. Thiel and S. S. Stahl, *Chem. Sci.*, 2017, **8**, 1282–1287.
3 H. P. L. Gemoets, Y. Su, M. Shang, V. Hessel, R. Luque and T. Noël, *Chem. Soc. Rev.*, 2015, **45**, 83–117.
4 M. O'Brien, I. R. Baxendale and S. V. Ley, *Org. Lett.*, 2010, **12**, 1596–1598.
5 J. S. Carey, D. Laffan, C. Thomson and M. T. Williams, *Org. Biomol. Chem.*, 2006, **4**, 2337–2347.
6 P. M. Osterberg, J. K. Niemeier, C. J. Welch, J. M. Hawkins, J. R. Martinelli, T. E. Johnson, T. W. Root and S. S. Stahl, *Org. Process Res. Dev.*, 2015, **19**, 1537–1543.
7 T. Tsubogo, H. Oyamada and S. Kobayashi, *Nature*, 2015, **520**, 329–332.
8 C. Wiles and P. Watts, *Green Chem.*, 2012, **14**, 38–54.
9 Y. Mo and K. F. Jensen, *React. Chem. Eng.*, 2016, **1**, 501–507.
10 A. Adamo, R. L. Beingessner, M. Behnam, J. Chen, T. F. Jamison, K. F. Jensen, J.-C. M. Monbaliu, A. S. Myerson, E. M. Revalor, D. R. Snead, T. Stelzer, N. Weeranoppanant, S. Y. Wong and P. Zhang, *Science*, 2016, **352**, 61–67.
11 J. Imbrogno, L. Rogers, D. A. Thomas and K. F. Jensen, *Chem. Commun.*, 2017, **54**, 70–73.
12 Y. Mo, H. Lin and K. F. Jensen, *Chem. Eng. J.*, 2018, **335**, 936–944.
13 N. Zaborenko, R. J. Linder, T. M. Braden, B. M. Campbell, M. M. Hansen and M. D. Johnson, *Org. Process Res. Dev.*, 2015, **19**, 1231–1243.
14 A. Constantinou, G. Wu, A. Corredera, P. Ellis, D. Bethell, G. J. Hutchings, S. Kuhn and A. Gavriilidis, *Org. Process Res. Dev.*, 2015, **19**, 1973–1979.
15 M. O'Brien, N. Taylor, A. Polyzos, I. R. Baxendale and S. V. Ley, *Chem. Sci.*, 2011, **2**, 1250–1257.
16 A. Polyzos, M. O'Brien, T. P. Petersen, I. R. Baxendale and S. V. Ley, *Angew. Chem., Int. Ed.*, 2011, **50**, 1190–1193.
17 I. Pinnau and L. G. Toy, *J. Membr. Sci.*, 1996, **109**, 125–133.
18 P. Bernardo, E. Drioli and G. Golemme, *Ind. Eng. Chem. Res.*, 2009, **48**, 4638–4663.
19 J. H. Lowry, J. S. Mendlowitz and N. S. (Mani) Subramanian, *Opt. Eng.*, 1992, **31**, 1982–1986.
20 P. R. Resnick and W. H. Buck, in *Fluoropolymers 2*, Springer, Boston, MA, 2002, pp. 25–33.
21 L. Yang and K. F. Jensen, *Org. Process Res. Dev.*, 2013, **17**, 927–933.
22 J. M. Hoover and S. S. Stahl, *J. Am. Chem. Soc.*, 2011, **133**, 16901–16910.
23 J. M. Hoover, B. L. Ryland and S. S. Stahl, *ACS Catal.*, 2013, **3**, 2599–2605.
24 J. M. Hoover, B. L. Ryland and S. S. Stahl, *J. Am. Chem. Soc.*, 2013, **135**, 2357–2367.
25 X. Ye, M. D. Johnson, T. Diao, M. H. Yates and S. S. Stahl, *Green Chem.*, 2010, **12**, 1180–1186.
26 J. E. Steves, Y. Preger, J. R. Martinelli, C. J. Welch, T. W. Root, J. M. Hawkins and S. S. Stahl, *Org. Process Res. Dev.*, 2015, **19**, 1548–1553.
27 J. F. Greene, Y. Preger, S. S. Stahl and T. W. Root, *Org. Process Res. Dev.*, 2015, **19**, 858–864.
28 C.-C. Chen, *Ind. Eng. Chem. Res.*, 2011, **50**, 10283–10291.
29 A. M. Polyakov, L. E. Starannikova and Y. P. Yampolskii, *J. Membr. Sci.*, 2004, **238**, 21–32.
30 A. M. Polyakov, L. E. Starannikova and Y. P. Yampolskii, *J. Membr. Sci.*, 2003, **216**, 241–256.

31 M. H. Al-Dahhan, F. Larachi, M. P. Dudukovic and A. Laurent, *Ind. Eng. Chem. Res.*, 1997, **36**, 3292–3314.
32 V. Holler, D. Wegricht, I. Yuranov, L. Kiwi-Minsker and A. Renken, *Chem. Eng. Amp. Technol.*, 2000, **23**, 251–255.
33 N. de Mas, A. Günther, T. Kraus, M. A. Schmidt and K. F. Jensen, *Ind. Eng. Chem. Res.*, 2005, **44**, 8997–9013.
34 M. Al-Rawashdeh, F. Yue, N. G. Patil, T. A. Nijhuis, V. Hessel, J. C. Schouten and E. V. Rebrov, *AIChE J.*, 2014, **60**, 1941–1952.